奥氏体不锈钢储能焊接头组织形成规律

徐 峰[1,2]， 徐锦锋[2]， 翟秋亚[2]
（1. 陕西理工学院 材料学院，陕西 汉中 723003；
2. 西安理工大学 材料学院，西安 710048）

徐 峰

摘 要：采用微型储能焊机对厚度为 0.2 mm 的 0Cr18Ni9 奥氏体不锈钢薄板进行了点焊连接研究，理论分析了微型熔核的温度场和冷却速率．结果表明，微型接头由熔核区和熔合区组成．极短的焊接时间，高的冷却速率 5.1× 10^6 K/s，使得熔核中奥氏体组织来不及长大，熔核凝固组织得到显著细化，具有快速凝固特征；同时，熔核中奥氏体组织在敏化温度区停留时间很短，抑制了铬在奥氏体晶界上的析出．当储能焊接电压为 80 V、电容为 6 600 μF、电极力为 18 N 时，可获得综合性能优良的高质量点焊接头．

关键词：奥氏体不锈钢；储能焊；点焊接头
中图分类号：TG142.71 文献标识码：A 文章编号：0253－360X(2009)12－0101－04

0 序 言

奥氏体不锈钢以其良好的耐蚀性、高强度和焊接性能，在航空航天、汽车、机械、仪器仪表、能源等工程领域得到广泛的应用．但由于奥氏体不锈钢热导率小，线膨胀系数大，普通熔化焊热输入大，加热时间长，易形成方向性很强的粗大柱状晶焊缝组织；而且热影响区宽度大，导致焊接接头力学性能恶化，难以保证焊接质量[1,2]．而储能焊具有焊接时间短（μs 级）、热影响区窄、焊接变形和残余应力小等优点，接头冷却速率高达 10^6 K/s，易获得组织细小、致密的高质量焊接接头[3－5]．为此，文中采用微型储能焊机对 0Cr18Ni9 奥氏体不锈钢薄板进行点焊连接，观察分析点焊接头形貌特征和组织形态，进而研究接头组织与性能之间的相关规律，为奥氏体不锈钢的快速凝固连接提供试验支持．

1 试验方法

试验用材料为 0Cr18Ni9 奥氏体不锈钢，焊接试样的尺寸为 10 mm×5 mm×0.2 mm 的薄板，是从厚度为 5 mm 的不锈钢热轧板材上经线切割加工而成．

试验用不锈钢薄板经金刚砂纸打磨、丙酮清洗后，装配成如图 1 所示的搭接接头．在微型电容储能焊机上进行点焊连接．焊接主要参数为储能焊接电压 U＝70～85 V，电容 C＝6 600 μF，电极力 F＝15～20 N．焊接能量、电压和电容之间的函数关系为 $E=CU^2/2$．因此，焊接能量在 16.17～23.84 J 之间．

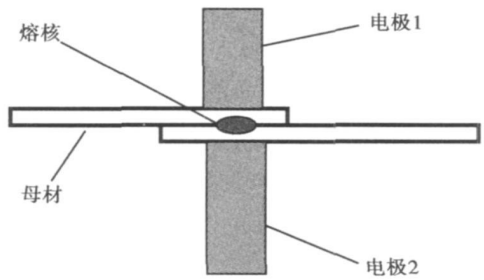

图 1 搭接接头示意图
Fig. 1 Scheme of lap joint

焊接接头试样经环氧树脂镶嵌成标准金相制样后，用王水浸蚀．应用 XJG －05 型光学显微镜观察分析接头形貌及其微观组织，应用 RigakvD －MAX25001PC 型 X 射线衍射仪分析熔核相组成，利用数字式 SH －500 推拉力计测试接头抗剪强度．

2 试验结果与分析

2.1 不锈钢点焊接头微观组织

0Cr18Ni9 奥氏体不锈钢储能点焊接头整体形貌如图 2a 所示．接头由两个区域组成，分别为熔核区

收稿日期：2009－05－25

与熔核向奥氏体基体过渡的熔合区. 熔核形状比较规则, 位于接头的中心部位, 约占接头总厚度的 2/3, 其组织为均匀细小的奥氏体等轴晶, 晶粒尺寸为 10 ~ 25 μm; 熔合区宽度较窄, 约 10 ~ 15 μm, 勾勒出熔核和母材之间的分界线, 其组织细小未发现缺陷, 晶粒尺寸约 7 ~ 11 μm, 如图 2b 所示. 由于熔合区冷却速率高于熔核区域, 由熔合区向熔核中心形成细密的柱状晶组织, 柱晶长度约 28 ~ 43 μm, 柱晶间距约 4 ~ 8 μm. 与熔合区毗邻的母材组织未发生明显的粗化, 与其原始组织仍然保持良好的一致性(图 2a). 可见, 储能焊可实现 0Cr18Ni9 奥氏体不锈钢薄板的点焊连接, 熔核与基体间熔合良好. 当焊接能量在 16.17 ~ 23.84 J 时, 可获得组织细小致密的高质量焊接接头.

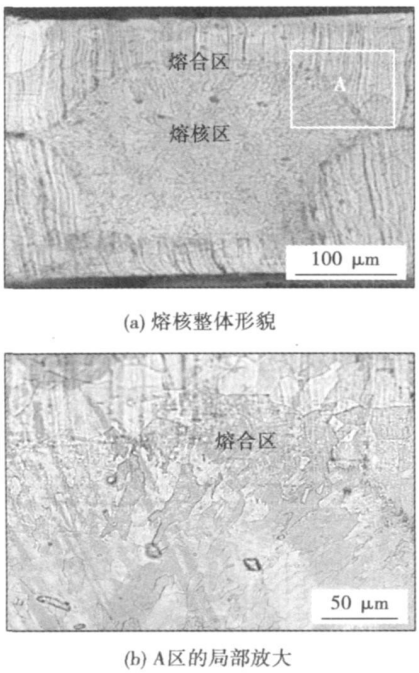

图 2 奥氏体不锈钢储能点焊熔核整体形貌

Fig. 2 Microstructure morphology of whole nugget by capacitor discharge welding

2.2 熔核金属的快速凝固过程分析

电容储能点焊利用电容瞬时放电产生的电流经电极加载在被焊板材上, 形成放电回路. 板材接触电阻瞬时产生的热量使得接触界面板材局部熔化形成熔核. 电容放电结束后, 由于铜电极和周围基体的快速吸热, 熔核处于较大的过冷状态, 熔核的冷却速率很大(10^6 K/s), 高的冷却速率使熔核的形核率显著增大, 从而形成细密的快速凝固组织. 为了揭示熔核组织的形成规律, 对熔核的温度场进行了理论计算. 为计算方便, 将熔核形状简化为球形, 并假设散热过程是向四周均匀进行的. 采用三维传热一维计算模型对熔核的温度场和冷却速率进行理论分析. 建立温度、空间和时间三维关系式为

$$T = T_0 + \frac{2(T_0 - T_1)R_0}{\pi R}\sum_{n=1}^{\infty}\frac{(-1)^n}{n}e^{\frac{n^2\pi^2\alpha^2}{R_0^2}t}\sin\frac{n\pi R}{R_0} \tag{1}$$

式中: $a^2 = \lambda/c\rho$, λ, c 和 ρ 分别为合金熔体的热导率、比热容和密度, $a^2 = 7.527\times10^{-5}$ Wm^2/J; t 为焊接时间, 取 350 μs; T_0 为环境温度, 取 300 K; T_1 为熔核的温度, 取 1 789 K; R_0 为熔核的最大半径, 此处为等积圆半径, 取 120 μm; R 为熔核半径. 理论计算获得熔核温度场如图 3 所示, 熔核冷却曲线如图 4 所示. 可以看出, 在熔核凝固初期、随着熔核半径的增大, 温度急剧下降. 熔核的热循环时间为 350 μs, 但熔核的凝固却主要集中在前 100 μs. 理论计算获得的熔核平均冷却速率高达 5.1×10^6 K/s, 熔核凝固时间极短仅为100 μs. 熔核的凝固过程具有快速凝

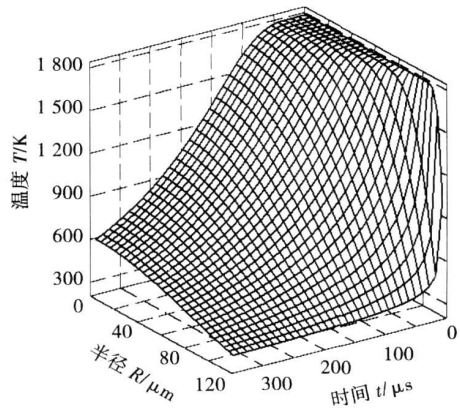

图 3 点焊接头熔核温度场

Fig. 3 Temperature field of spot-welding joint

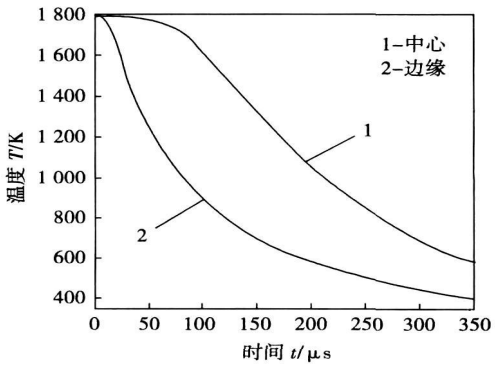

图 4 点焊接头熔核冷却曲线

Fig. 4 Cooling curves of spot-welding joint

固特征.

由于电容储能点焊冷却速率大，熔核金属于瞬间熔化后，便即刻进入急冷快速凝固阶段，发生奥氏体的瞬间形核与快速生长，形成熔核中的细小致密等轴晶组织，从而避免了因偏析导致的焊接接头性能降低现象的发生，保证了焊接质量.

在常规焊接工艺下，奥氏体不锈钢在加热到 450～850 ℃温度区间易发生过饱和碳向奥氏体晶粒边界扩散，并与晶界的铬化合形成碳化铬($Cr_{23}C_6$)的现象. 由于铬在奥氏体中的扩散速度小于碳的扩散速度，使晶界的铬得不到及时补充，造成奥氏体边界贫铬. 当晶界附近的金属铬含量低于 12%时，就失去了抗腐蚀能力，容易产生晶间腐蚀，在受到应力时即会沿晶界断裂，几乎完全丧失强度[6－9]. 而电容储能焊接热过程持续时间极短，能抑制上述 C 与 Cr 元素的扩散和聚集，不会在晶界处形成贫铬区，从而预防了晶间腐蚀的发生. 更为关键的是，高的冷却速率使奥氏体不锈钢焊接过程中在敏化温度区间滞留时间极短，接头发生脆化的机率大大降低. X 射线衍射分析结果表明，焊接接头以奥氏体为主要组成相，其次是铁素体相和微量的其它相，没有碳化铬($Cr_{23}C_6$)形成，如图 5 所示. 可见，利用储能电容快速放电产生的能量不仅能够实现奥氏体不锈钢的焊接，而且避免了焊接接头晶界铬的析出，提高了奥氏体焊接性能，降低缺陷产生的几率，从而保证了奥氏体不锈钢储能焊焊接接头的使用性能.

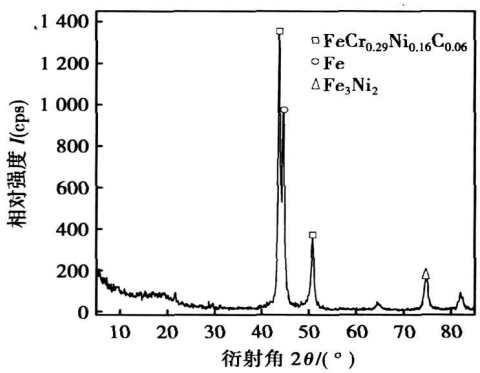

图 5　奥氏体不锈钢储能焊熔核 XRD 图谱

Fig. 5　XRD spectrum and microstructure of austenitic stainless steel nugget

2.3　焊接接头抗剪强度

点焊接头的抗剪强度主要取决于电极力、储能焊接电压和焊接能量等工艺参数. 在电极力作用下熔核周围金属会发生塑性变形和强烈的再结晶而形成先于熔核生长的塑性环，对消除焊点缺陷、改善金属组织和提高力学性能具有较大作用. 而电压对焊接能量有直接的影响，焊接能量过小，被焊材料不能被加热到热塑性状态；而焊接能量过大很容易产生喷溅和击穿，很难得到高力学性能的接头. 通过试验发现当储能焊接电压一定时，随着电极力的增加，接头抗剪强度也随之增加. 当电极力达到 18 N 时，抗剪强度达到最大值 116.8 MPa，进一步增加电极力，接头强度开始逐渐降低，如图 6 所示. 通过综合分析抗剪强度与焊接工艺参数之间的相关性发现，对于 0.2 mm 厚的 0Cr18Ni9 奥氏体不锈钢，当焊接电容为6 600 μF、储能焊接电压为 80 V、电极力为 18 N 时，可获得综合性能优良的焊接接头.

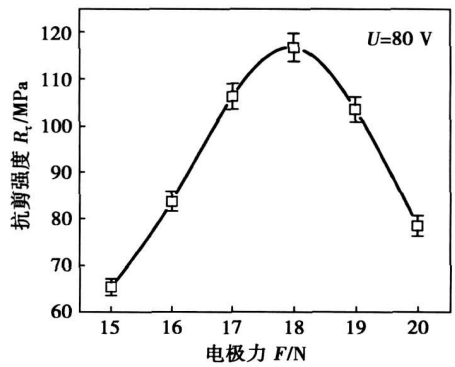

图 6　接头抗剪强度随电极力的变化曲线

Fig. 6　Variation of shear strength of joint with electrode force

3　结　　论

(1) 微型接头由熔核及熔合区组成. 熔核厚度约占接头厚度的2/3，组织为奥氏体和奥氏体晶界上分布的少量铁素体组成，其向基体金属过渡良好.

(2) 在储能焊条件下接头冷却速率平均高达 10^6 K/s，接头组织具有明显的快速凝固特征，同时接头在敏化温度区停留时间很短，避免了铬在奥氏体晶界上的析出. 焊缝组织细小致密，保证了接头的使用性能.

(3) 对于 0.2 mm 厚的 0Cr18Ni9 奥氏体不锈钢薄板的储能焊，当储能焊接电压为 80 V、电容为 6 600 μF、电极力为 18 N 时，抗剪强度可达 116.8 MPa，获得综合性能优良的高质量焊接接头.

参考文献：

[1]　王希靖，叶结和，孙丙岩，等. 0Cr18Ni9 不锈钢搅拌摩擦焊接头的微观组织和性能[J]. 热加工工艺，2006，35(23)：36－39.

Wang Xijing, Ye Jiehe, Sun Bingyan, *et al*. Microstructure and mechanical properties of friction stir weld joint of 0Cr18Ni9 stainless steel [J]. Hot Working Technology, 2006, 35(23): 36—39.

[2] 中国机械工程学会焊接学会. 焊接手册第 2 卷(第 2 版)[M]. 北京: 机械工业出版社, 2001.

[3] 李明高, 邱小明, 孙大千, 等. TiNi 形状记忆合金与不锈钢的储能焊[J]. 轻金属, 2005(7): 57—59.
Li Minggao, Qiu Xiaoming, Sun Daqian, *et al*. Study on capacitor discharge welding of TiNi shape memory alloy and stainless steel[J]. Light Metal, 2005(7): 57—59.

[4] Xu Jinfeng, Zhai Qiuya, Yuan Sen, *et al*. Energy-storage welding connection characteristics of AZ91D magnesium alloy rapid solidification ribbons[J]. Journal of Materials Science and Technology, 2004, 20(4): 431—433.

[5] 雷 鸣, 翟秋亚, 徐锦锋, 等. Al_2O_3F/ADC12 复合材料储能焊接头组织形成规律[J]. 焊接学报, 2007, 28(4): 101—104.
Lei Ming, Zhai Qiuya, Xu Jinfeng, *et al*. Microstructural formation of Al_2O_3 fiber reinforced Al-matrix composites joint by capacitor discharge welding[J]. Transactions of the China Welding Institution, 2007, 28(4): 101—104.

[6] 张心保, 王志斌, 赵春林, 等. 热输入对 00Cr12NiTi 不锈钢焊接 HAZ 组织及性能的影响[J]. 焊接, 2008(3): 66—68.
Zhang Xinbao, Wang Zhibin, Zhao Chunlin, *et al*. Effect of heat input on microstucture and mechanical properties of HAZ in welded joint of 00Cr12NiTi ferrite stainless steel[J]. Welding & Joining, 2008(3): 66—68.

[7] Suutala N. Effect of solidification conditions on the solidification mode in austenitic stainless steels[J]. Metallurgical Transactions A, 1983, 14A(2): 191—193.

[8] 秦 斌, 王宝森. 焊接速度对奥氏体不锈钢接头性能的影响[J]. 钢铁钒钛, 2008, 29(2): 51—53.
Qin Bin, Wang Baosen. Effect of welding velocity on properties of welding joint of austenitic stainless steel[J]. Iron Steel Vanadium Titanium, 2008, 29(2): 51—53.

[9] 张文钺. 焊接冶金学[M]. 北京: 机械工业出版社, 2005.

作者简介: 徐 峰, 男, 1977 年出生, 硕士研究生, 讲师. 主要从事先进材料及其焊接研究. 发表论文 5 篇.

Email: xf96050@163.com

[上接第 68 页]

thermal cycling and thermal shock testing for board level reliability of soldered interconnections[J]. Microelectronics Reliability, 2007, 47(2—3): 444—449.

[2] 李晓延, 严永长, 史耀武. 金属间化合物对 SnAgCu/Cu 界面破坏行为的影响[J]. 机械强度, 2005, 27(5): 666—671.
Li Xiaoyan, Yan Yongchang, Shi Yaowu. Influence of IMC on the interface failure of tin-silver-copper solder joints[J]. Journal of Mechanical Strength, 2005, 27(5): 666—671.

[3] 盛 重, 薛松柏, 张 亮, 等. 基于蠕变模型倒装芯片焊点疲劳寿命预测[J]. 焊接学报, 2008, 29(10): 53—56.
Sheng Zhong, Xue Songbai, Zhang Liang, *et al*. Fatigue life prediction for flip chip soldered joints based on creep stain model[J]. Transactions of the China Welding Institution, 2008, 29(10): 53—56.

[4] Perkins A, Sitaraman S. Vibration-induced solder joint failure of a ceramic column grid array (CCGA) package[C] // Electronic Components and Technology Conference, Atlanta, GA, USA, 2004: 1271—1278.

[5] Li X Y, Wang Z S. Thermo-fatigue life evaluation of SnAgCu solder joints in flip chip assemblies[J]. Journal of Materials Processing Technology, 2007, 183(1): 6—12.

[6] Kim J W, Jung S B. Design of solder joint structure for flip chip package with an optimized shear test method[J]. Journal of Electronic Materials, 2007, 36(6): 690—696.

[7] Pang J H L, Seetoh C W, Wang Z P. CBGA solder joint reliability evaluation based on elastic-plastic-creep analysis[J]. Journal of Electronic Packaging, 2000, 122(3): 255—261.

[8] 周 祥, 祝新军, 马孝松. PCB 粘弹性对 QFN 焊点可靠性的影响[J]. 电子元件与材料, 2008, 27(4): 69—72.
Zhou Xiang, Zhu Xinjun, Ma Xiaosong. Effect of viscoelasticity of PCB on solder joints reliability of QFN[J]. Electronic Components and Materials, 2008, 27(4): 69—72.

[9] Qian Z F, Liu S. On the life prediction and accelerated testing of solder joints[J]. International Journal of Microcircuits and Electronic Packaging, 1999, 22(4): 289—304.

作者简介: 盛 重, 男, 1984 年出生, 硕士研究生. 主要从事微电子焊接及无铅钎料研究. 已发表论文 4 篇.

Email: orochiai@126.com

Numerical simulation of slit type cracking test for 9% Ni steel

BAI Shiwu[1,2], LI Wushen[1], YAN Chunyan[1,3], YIN Zhanghua[2], HUANG Fuxiang[2] (1. School of Materials Science and Engineering, Tianjin University, Tianjin 300072, China; 2. Petroleum-Gas Pipeline Research Institute of China, Langfang 065000, China; 3. College of Mechanical and Electrical Engineering, Hohai University, Changzhou 213022, China). p 93—96

Abstract: With SYSWELD software, the temperature and stress field of 9% Ni steel Y-slit weldments with different preheat temperatures were simulated by applying double-ellipsoid heat source. Distribution laws of welding temperature and stress field were studied. Effects of preheat temperature on welding heat cycles and residual stress were analyzed. Results show that with increasing preheat temperature, cooling rate decreases facilitates escaping of hydrogen and self-tempering of martensite, the average stress level and cold-cracking susceptibility of the weldments increase, so high preheat temperature shall be avoided for 9%Ni steel welding.

Key words: 9% Ni steel; slit type cracking test; preheat temperature; temperature field; stress field

Analysis on heat-affected zone toughness of railroad freight TCS345 stainless steel weld joints

WANG Baosen, MA Zhaohui, ZHU Shuangchun, XU Ke (Research Institute, Baosteel Iron & Steel Co. Ltd, Shanghai 201900, China). p 97—100

Abstract: The transformation temperature phase diagram of 12% chromium steel is obtained by using Thermal-cal software. Process of welding 12% chromium stainless steel is analysed with the phase transformation temperature scope. The heat-affected zone (HAZ) of the weld joints is observed with optic microscope and scanning electronic microscope, which the microstructure consists of ferrite, martensite, coarse grain heat-affected zone (CGHAZ), fine grain heat-affected zone (FGHAZ) and Ti(C/N). The key elements that affect toughness of CGHAZ are ferritic grain size and martensitic content. The base material has the best impact toughness when grain size of Ti(C/N) reaches 2—5 μm. The lowest ductility-brittle transition temperature in CGHAZ is —22 ℃ when content of carbon plus nitrogen in base material is about 0.02% and martensitic content in CGHAZ is 40% under some certain welding procedure.

Key words: chromium ferritic stainless steel; coarse grain heat affected zone; impact toughness

Microstructural formation of austenitic stainless steel joint by capacitor discharge welding

XU Feng[1,2], XU Jinfeng[2], ZHAI Qiuya[2] (1. School of Materials Science and Engineering, Shaanxi University of Technology, Hanzhong 723003, China; 2. Xi'an University of Technology, Xi'an 710048, China). p 101—104

Abstract: The 0Cr18Ni9 austenitic stainless steel sheet with 0.2 mm thickness was welded in capacitor discharge spot welding. The temperature field and cooling rate of nugget was calculated. The results show that the joint microstructure consists of nugget zone and semi-melt zone. Due to very short time in welding, the cooling rate of the joint reaches to 5.1×10^6 K/s, the growth of austenite microstructure is impeded, and the microstructure of the nugget is refined, which has rapidly solidified characteristics. As the austenite microstructure of the nugget stays in temperature province of activation with very short time, the chrome of austenite grain boundary precipitations is checked. To obtain the high quality spot-weld joint, the welding parameters are determined as: welding voltage 80 V, capacitor 6 600 μF and electrode pressure 18 N.

Key words: austenitic stainless steel; capacitor discharge welding; spot-weld joint

Analysis for the influences of aluminum alloy P-MIG welding parameters on welding arc

LU Zhiqiang[1,2], HUA Xueming[1,2], LI Fang[1,2], WU Yixiong[1,2] (1. Material and Science Engineering Department, Shanghai Jiaotong University, Shanghai 200240, China; 2. The Key Laboratory of Laser Processing and Material Modification of Shanghai, Shanghai 200240, China). p 105—108

Abstract: Under the same average welding current and welding voltage, by regulating the different based current and peak current, the Al-Mg alloy was welded with Al-Mg filler wire. The photos of welding arc were obtained by using high-speed video photography. Peak current has great influence on the shape and characteristics of the arc. With increasing the peak current value, rotated arc appears and pulsed rotated metal transfer behavior occurs. Based current has little influence on the arc shape. Base current is the important parameter for keeping arc burning. At pulse off time, it must be given base current value which is large enough to keep the arc burning stably. In this study, the arc shape is defined by arc length, arc width and arc portrait cross-section area, which will be influenced by the weld current. Peak current is important parameter of arc temperature and pulse energy. The study shows that when the arc is burning at pulse on time, the arc length, arc width and arc portrait cross-section area increase with raising peak current.

Key words: aluminum alloy; arc shape; pulsed-insert gas welding; current

Welding technology and microstructure of MIG welded magnesium alloy

WANG Peng, SONG Gang, LIU Liming (School of Materials Science and Engineering, Dalian University of Technology, Dalian 116024, China). p 109—112

Abstract: The pulsed MIG welding was used to weld AZ31B Mg alloy, and the weldability of the alloy was studied. The microstructure, mechanical property and hardness of the welded joint were investigated via the metal phase microscopy, scanning electron microscope, tensile testing machine and hardness instrument. The results show that one-side welding with back can be obtained through this technique at optimized parameters when there was no groove and no shaped ban, which continuous butt joints have no surface defects. The heat-affected zone of the joints is narrow, and the grains of the zone are slightly larger than that of the base metal. The grains of fusion zone are tiny, the microstructure is homogeneous and the hardness of welded joint is higher than that of the base metal. The tensile strength is up to 95% of the base metal.

Key words: pulsed MIG welding; magnesium alloy; welding process; microstructure